the Mauna Kea observations of 24 August 1989.
11. K. H. Baines and W. H. Smith, in preparation.
12. G. L. Tyler *et al.*, *Science* **246**, 1466 (1989).
13. H. N. Russell, *Astrophys. J.* **43**, 173 (1916).
14. Radii were based on information furnished by the Voyager Imaging Team in advance of publication (J. Gougen and P. Thomas, personal communication).
15. R. M. Nelson *et al.*, *J. Geophys. Res.* **92**, 14905 (1987).
16. B. W. Hapke, *Icarus* **67**, 264 (1986).
17. B. J. Buratti and J. Veverka, *ibid.* **58**, 254 (1984).
18. L. M. Trafton, in *Uranus and Neptune*, J. T. Bergstralh, Ed., NASA CP 2330, 481 (1984).
19. J. Lunine and D. Stevenson, *Nature* **317**, 238 (1985).
20. J. A. Stansberry, *Geophys. Res. Lett.* **16**, 961 (1989).
21. A. P. Zent *et al.*, *ibid.*, p. 965.
22. S. Stern, *ibid.*, p. 981.
23. O. Franz, *Icarus* **45**, 602 (1981).
24. N. Lark *et al.*, *ibid.* **79**, 239 (1989).
25. B. J. Buratti and J. Veverka, *ibid.* **51**, 93 (1983).
26. J. E. Colwell *et al.*, *ibid.*, in press.
27. P. D. Nicholson *et al.*, in preparation.
28. W. B. Hubbard *et al.*, *Nature* **319**, 636 (1986).
29. C. E. Covault *et al.*, *Icarus* **67**, 126 (1986).
30. J. N. Cuzzi, *ibid.* **63**, 312 (1985).
31. L. J. Horn *et al.*, *ibid.* **76**, 485 (1988).
32. B. A. Smith *et al.*, *Science* **212**, 163 (1981).
33. B. A. Smith *et al.*, *ibid.* **233**, 43 (1986).
34. R. G. French *et al.*, *Icarus* **67**, 134 (1986).
35. T. G. Brophy, L. W. Esposito, G. R. Stewart, *Bull. Am. Astron. Soc.* **21**, 932 (1989).
36. P. Goldreich and S. Tremaine, *Annu. Rev. Astron. Astrophys.* **20**, 249 (1982).
37. M. R. Showalter and J. A. Burns, *Icarus* **52**, 526 (1982).
38. R. A. Kolvoord and J. A. Burns, *Bull. Am. Astron. Soc.* **20**, 859 (1988).
39. L. W. Esposito and J. Colwell, *Nature* **339**, 605 (1989).
40. The Neptune pole used in the ring range calculations was right ascension = 298.7924°, declination = 42.8482°. The Voyager Navigation Team trajectory solution used was NAV K.1.
41. With the completion of the Voyager 2 Grand Tour, the PPS Team acknowledges with heartfelt thanks all the members of the Voyager Flight Team who worked so diligently to enable the PPS to have encounters with Jupiter, Saturn, Uranus, and Neptune, which were so filled with marvelous scientific results. To all those people, past and present, we owe a debt of immeasurable gratitude. The PPS team also remembers fondly J. Long and C. Stembridge, who, though no longer with us in body, were with us in spirit during this encounter. We also thank P. D. Nicholson and R. French for many helpful conversations as well as numerous geometry computations during the time period when each new pre-encounter satellite observation tweaked our knowledge of the Neptunian pole direction. The PPS team wishes to thank M. Morrison, S. Kuo, J. Hui, A. Graps, and B. Hapke for their help during the active Neptune encounter period. The continuing support of the NASA Office of Solar System Exploration is gratefully acknowledged. This work was support under NASA contracts to J.P.L. and the University of Colorado.

2 November 1989; accepted 15 November 1989

Infrared Observations of the Neptunian System

B. CONRATH, F. M. FLASAR, R. HANEL, V. KUNDE, W. MAGUIRE, J. PEARL, J. PIRRAGLIA, R. SAMUELSON, P. GIERASCH, A. WEIR, B. BEZARD, D. GAUTIER, D. CRUIKSHANK, L. HORN, R. SPRINGER, W. SHAFFER

The infrared interferometer spectrometer on Voyager 2 obtained thermal emission spectra of Neptune with a spectral resolution of 4.3 cm^{-1}. Measurements of reflected solar radiation were also obtained with a broadband radiometer sensitive in the visible and near infrared. Analysis of the strong C_2H_2 emission feature at 729 cm^{-1} suggests an acetylene mole fraction in the range between 9×10^{-8} and 9×10^{-7}. Vertical temperature profiles were derived between 30 and 1000 millibars at 70° and 42°S and 30°N. Temperature maps of the planet between 80°S and 30°N were obtained for two atmospheric layers, one in the lower stratosphere between 30 and 120 millibars and the other in the troposphere between 300 and 1000 millibars. Zonal mean temperatures obtained from these maps and from latitude scans indicate a relatively warm pole and equator with cooler mid-latitudes. This is qualitatively similar to the behavior found on Uranus even though the obliquities and internal heat fluxes of the two planets are markedly different. Comparison of winds derived from images with the vertical wind shear calculated from the temperature field indicates a general decay of wind speed with height, a phenomenon also observed on the other three giant planets. Strong, wavelike longitudinal thermal structure is found, some of which appears to be associated with the Great Dark Spot. An intense, localized cold region is seen in the lower stratosphere, which does not appear to be correlated with any visible feature. A preliminary estimate of the effective temperature of the planet yields a value of 59.3 ± 1.0 kelvins. Measurements of Triton provide an estimate of the daytime surface temperature of 38^{+3}_{-4} kelvins.

DURING THE VOYAGER 2 ENCOUNTER, the infrared interferometer spectrometer (IRIS) obtained thermal emission and reflected solar radiation measurements of Neptune and Triton. The dual instrument consists of a Michelson interferometer operating in the thermal infrared with a spectral resolution of 4.3 cm^{-1} and a single-channel radiometer sensitive to reflected sunlight between 0.4 and 1.5 μm. Both components share a 50-cm Cassegrain telescope with a common circular field of view of 0.25° full cone angle. The interferometer is calibrated by scaling the spectra of the observed object to that of deep space while maintaining the instrument at 200 K. Occasional measurements of reflected sunlight from a diffuse reflector carried on the spacecraft are used to calibrate the radiometer. The instrument and its characteristics have been described in detail elsewhere (*1*), and results obtained for the Jovian, Saturnian, and Uranian systems have been presented (*2–6*). In this report we describe preliminary results obtained for Neptune and Triton.

Thermal emission spectra of Neptune. Because of the very low temperatures encountered on Neptune, a signal-to-noise ratio greater than unity is achieved in individual spectra only in the spectral region between 200 and 320 cm^{-1}. Therefore, for most applications it is necessary to either use an average of several spectra or to integrate over broad intervals within individual spectra, or both. With this limitation in mind, observational sequences were designed and implemented that would provide adequate numbers of spectra to permit specific objectives to be met. Averages of several tens of spectra allow a useful effective signal-to-noise ratio to be achieved between 200 and 400 cm^{-1}, whereas averages of several hundred spectra permit analyses of selected spectral regions at higher wavenumbers to be carried out.

In Fig. 1 the spectrum corresponding to 70°S is an average of 390 individual spectra and that for 42°S is an average of 108 spectra. The Neptune spectrum over the wavenumber range shown is dominated by the S(0) collision-induced absorption line of H_2, which is centered at 354 cm^{-1}. The dominant factors that determine the behavior of the spectrum are the variation of atmospheric temperature with height and

B. Conrath, F. M. Flasar, R. Hanel, V. Kunde, W. Maguire, J. Pearl, J. Pirraglia, R. Samuelson, Laboratory for Extraterrestrial Physics, Goddard Space Flight Center, Greenbelt, MD 20771.
P. Gierasch and A. Weir, Astronomy Department, Cornell University, Ithaca, NY 14853.
B. Bezard and D. Gautier, Paris Observatory, 92190 Meudon, France.
D. Cruikshank, Ames Research Center, Moffett Field, CA 94035.
L. Horn and R. Springer, Jet Propulsion Laboratory, Pasadena, CA 91109.
W. Shaffer, Department of Meteorology, University of Maryland, College Park, MD 20472.

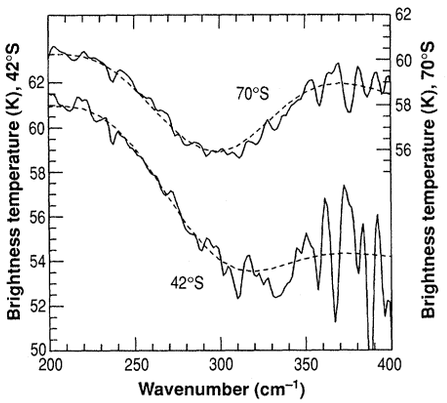

Fig. 1. Measured brightness temperature spectra of Neptune (solid curves) compared with theoretical spectra (broken curves) calculated from retrieved temperature profiles. The spectrum for 70°S is an average of 390 individual measurements with a mean emission angle of 43°. That at 42° is an average of 108 individual spectra with a mean emission angle of 22°. The difference in the shapes of the two spectra is a consequence of differences in the lower stratospheric temperatures at the two locations as well as the differences in the emission angles of the observations. For clarity, the 70°S spectrum is displaced upward 2 K, and its scale is shown on the right-hand side of the figure.

the emission angle at which the measurements were made. The data near 70°S were taken at a relatively high emission angle of 43°, and the increase in brightness temperature beyond 300 cm^{-1} near the line center results from an increase in atmospheric temperature with height in the lower stratosphere (*6a*). A smaller increase in brightness temperature near the line center is observed in the 42°S spectrum because the emission angle in this case was only 22°. Other factors that can affect the detailed shape of the spectrum in this region include the atmospheric helium abundance, the H_2 ortho-para ratio, the methane abundance, and clouds and hazes. It is possible in principle to obtain information on all of these atmospheric parameters through analyses of the spectra. To achieve unique solutions, however, it is usually necessary to invoke additional constraints, either from other measurements or from physical assumptions.

Helium abundance. Determination of the He abundance in the atmospheres of the giant planets is a major objective of the Voyager mission. Previous analyses of Voyager data have yielded He mole fractions of 0.10 ± 0.03 for Jupiter, 0.04 ± 0.02 for Saturn, and 0.15 ± 0.03 for Uranus (*7*). These results suggest that, relative to the solar abundance of the elements, Uranus shows no He depletion, Jupiter may be somewhat depleted, and Saturn is strongly depleted (*8*). Before the Voyager 2 encounter, the He abundance in the atmosphere of Neptune was not constrained observationally. Now that the necessary Voyager Neptune data have been acquired, it is possible to complete the study of He in the four outer planets.

If cloud opacity is minimal, an analysis of the shape of the infrared spectrum measured by Voyager IRIS provides one means of placing limits on the atmospheric He abundance. This type of analysis has previously been applied to the IRIS measurements of Uranus (*6*). Until it is verified that cloud opacity does not have a significant effect on the observed spectrum, however, it is not legitimate to apply this method to Neptune.

Alternatively, a comparison of IRIS data with Radio Science Subsystem data provides a potentially more sensitive method of achieving the same goal. If the opacity of clouds and hazes is not negligible, this comparison provides the only method. Systematic modeling implies that if methane ice is the sole source of cloud opacity, it should be possible to obtain a He mole fraction for Neptune comparable in accuracy to those obtained for the other outer planets. Preliminary analysis suggests a value within a factor of 1.5 of that for Uranus; until ongoing analysis provides a more accurate figure, we adopt the Uranus mole fraction of 0.15 in our data interpretation. In addition, we assume an equilibrium H_2 ortho-para ratio and neglect cloud opacity effects. Further analysis may modify these values.

Acetylene abundance. Reducing atmospheres that contain methane (CH_4) are also expected to have small amounts of hydrocarbons produced by photochemical reactions. Indeed, acetylene (C_2H_2) and ethane (C_2H_6) have been identified on Neptune from ground-based data (*9–12*). An average of 2300 individual Voyager infrared spectra selected from data with near normal viewing confirms the presence of C_2H_2 on Neptune (Fig. 2). The strong emission feature at 729 cm^{-1} is identified as the Q branch of the ν_5 band of C_2H_2. The emission peak is eight times the effective root mean square (RMS) noise level for the average spectrum. A determination of the actual C_2H_2 abundance is more difficult because it also requires a precise knowledge of stratospheric temperatures between approximately 0.01 and 5 mbar. The temperature range derived from the collision-induced H_2 spectrum covers the region from 30 to 1000 mbar and cannot be extrapolated reliably to lower pressures. In the future it may be possible to improve our knowledge of the temperature over the desired pressure range by using radio occultation data. For a preliminary analysis we used the temperature estimate of Orton *et al.* (*11*) to obtain a value for the C_2H_2 mole fraction. In the computation of the theoretical emission spectra we have assumed several uniform mixing ratios above a condensation level near 4 mbar, along with the normal temperature profile of Orton *et al.* (*11*). On the basis of a best fit to the measured spectrum, as shown in Fig. 2, the mole fraction is estimated to be $2.7 \pm 0.8 \times 10^{-7}$. The quoted error bar only accounts for the instrument noise. Considering the extreme "warm" and "cold" profiles proposed by Orton *et al.* (*11*), which reflect present uncertainties in the thermal structure, the probable error is substantially increased, and we obtain an estimate of the C_2H_2 mole fraction between 9×10^{-8} and 9×10^{-7}. These limits are consistent with ground-based analyses (*11, 12*). In our best-fit atmospheric model, most of the C_2H_2 emission originates from the 0.03 to 2.5-mbar region with the maximum contribution from the 1.5-mbar level.

The production of C_2H_2 in the atmosphere of Neptune most likely occurs through photolysis of both C_2H_6 and ethylene (C_2H_4), which in turn originate from CH_4 photodissociation occurring near the CH_4 homopause (*13, 14*) at pressures of one microbar or less. The C_2H_2 concentration profile then results from a balance between photochemical production and losses due to photolysis and condensation processes. Photochemical models predict average C_2H_2 mixing ratios of the order of 6×10^{-7} (*13*) and 1×10^{-7} (*14*) near 1.5 mbar, in agreement with the present determination.

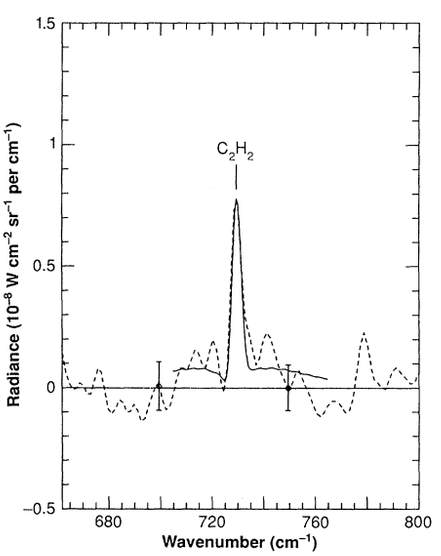

Fig. 2. Comparison of measured (broken curve) and calculated (solid curve) spectra in the vicinity of the ν_5 absorption band of C_2H_2. The measured spectrum is an average of 2300 individual spectra selected within the latitude range between 10° and 50°S. The theoretical spectrum is based on a line-by-line calculation, assuming a stratospheric C_2H_2 mole fraction of $2.7\ 10^{-7}$. The bars indicate the 1σ effective noise level for the average.

Temperatures and zonal winds. Because of the weak thermal emission from Neptune, it is necessary to form averages of 100 or more spectra in order to obtain a sufficient signal-to-noise ratio to perform a complete temperature profile retrieval. For this purpose, ensembles of spatially resolved spectra were obtained at 70° and 42°S, and 30°N. The averages of these spectra were inverted to obtain the profiles shown in Fig. 3, by means of techniques previously described (*15*). The spectral region between 200 and 400 cm^{-1} was used for this purpose, providing useful information between approximately 30 and 1000 mbar. At 70°S the lower stratosphere is found to be significantly warmer than at the other two locations, while at 30°N the atmosphere is relatively warm at pressures greater than 200 mbar. However, preliminary pointing information has been used in this analysis, and the results may be subject to some modification when the emission angles are better known; this is especially true of the profile at 30°N where the emission angle exceeds 50° and the sensitivity to this parameter is strong. In addition, the contribution of clouds to the infrared opacity, particularly at the lower atmospheric levels, has not been fully assessed, and the retrieved temperatures given here have neglected it.

Even though the retrieval of vertical temperature profiles from individual or small averages of spectra is precluded, it is still possible to obtain information on the mean temperature over broad atmospheric layers

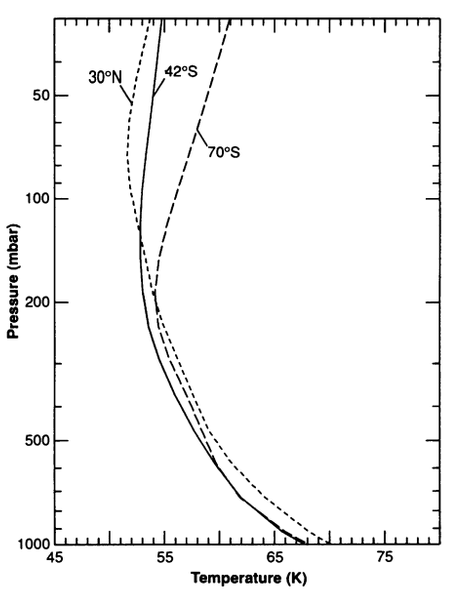

Fig. 3. Atmospheric profiles obtained by inversion of spectra at selected locations on Neptune. Measurements between 200 and 400 cm^{-1} within the S(0) collision-induced hydrogen lines were used in the retrievals. The region of maximum information for this spectral region lies between 30 and 1000 mbar.

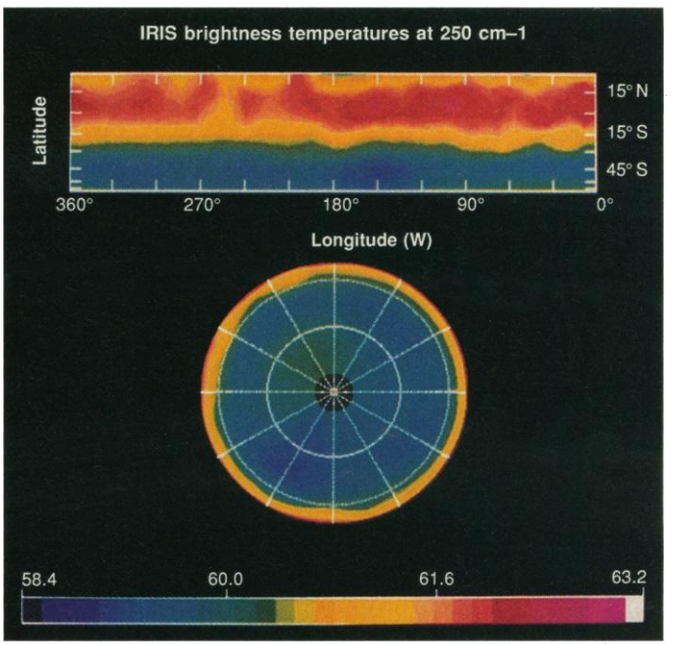

Fig. 4. Temperature maps of Neptune (at bottom of figure, calibrated in kelvins) at 250 cm^{-1} both in cylindrical geometry and as viewed from the south pole. The temperatures were spatially smoothed by means of a Gaussian weighting with full width at half-maximum equal to the projected instrument field of view.

from individual spectra. Second-order polynomials were fit to the spectra over the range of 200 to 300 cm^{-1} and 300 to 450 cm^{-1}. The fitted brightness temperatures at 250 and 350 cm^{-1} were then adjusted to normal viewing for a fixed (equatorial) gravitational acceleration by limb functions that were computed for the 70°S temperature profile. At normal viewing these brightness temperatures correspond, respectively, to the atmospheric temperature in the lower troposphere averaged between 300 and 1000 mbar, and in the lower stratosphere averaged between 30 and 120 mbar. In this manner the brightness temperatures at 250 and 350 cm^{-1} were converted to temperatures on isobars over the globe. This procedure is similar to that described in greater detail elsewhere (*6, 16*), and its validity rests on the assumption that the lapse rate in temperature varies little with horizontal location. The lapse rates do vary with latitude, particularly in the stratosphere, above the temperature minimum (Fig. 3). However, the shift in brightness temperatures from vertical viewing to viewing at an angle of 70°, which comprises the range of emission angles in the maps we used, differs by only 1 K at 350 cm^{-1} and 0.7 K at 250 cm^{-1} among the profiles shown. The actual horizontal thermal contrast in brightness temperature is several times greater.

Maps of normalized brightness temperatures were obtained from a sequence of observations in which the instrument continuously scanned Neptune from north to south along the subspacecraft meridian for a period of 20 hours. Because the subspacecraft latitude during this sequence was 23°S, the maps only cover latitudes from 30°N to 80°S. The field of view projected at the subspacecraft point subtends about 20° in latitude, but the spacing between footprints is only one-half of that. The sequence of observations was such that radiances observed at a given latitude should all have the same emission angle; hence errors in the limb correction can cause errors in the inferred meridional temperature contrast but not in the zonal contrast. Figs. 4 and 5 display the brightness temperatures at 250 and 350 cm^{-1}, respectively. The temperature variation is approximately twice as large at 350 cm^{-1} as it is at 250 cm^{-1}. The dominant features in both maps are the broad warm band at low latitudes and the broad cold band at mid-southern latitudes. However, the zonal variation of temperature (that is, along latitude circles) is quite marked, much greater than that observed on Uranus (*6, 16*) or on Saturn (*4*), and it is most nearly similar to that observed on Jupiter (*3*). In both the warm and cold bands, there is a suggestion of a periodicity with wavenumber 5 or 6. The observations were made on the nightside of Neptune, but attempts have been made to correlate the distinct thermal features with those observed at visible wavelengths by estimating their longitudes from the rotation periods determined by Voyager imaging observations (*17*). So far, these attempts have not yielded any identifiable correlation. For example, one of the most distinct features in the maps is the cold anomaly at 40°S, 75°W in the 350 cm^{-1} map. It is not evident in the 250 cm^{-1} map. This is reminiscent of the Great Red Spot of Jupiter, which was quite distinct as a cold anomaly in the tropopause region and lower stratosphere, but was "in-

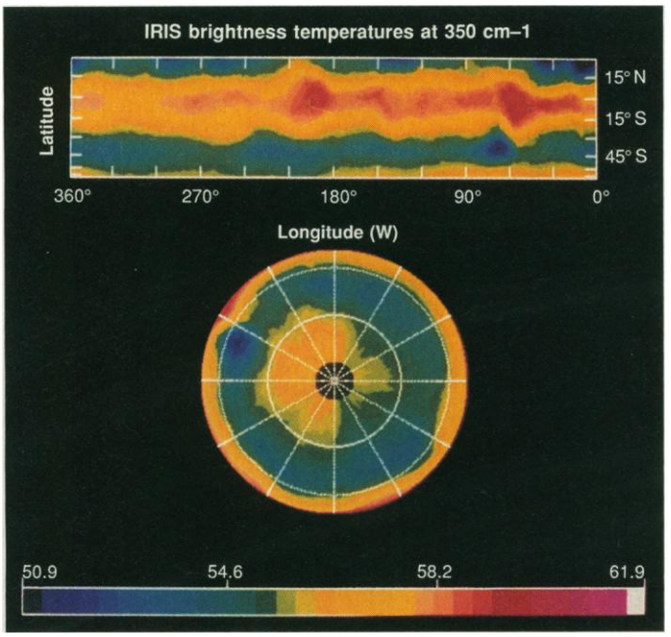

Fig. 5. Temperature maps as in Fig. 4 but at 350 cm^{-1}.

visible" in the lower troposphere at 500 mbar (*3, 18*). An obvious visible-feature candidate for the cold spot is the "Scooter," situated at 42°S. However, at the time of the mapping it was situated west of the anomaly, at 110°W. The predicted position of the visible feature "D2," at latitude 53°S, is more uncertain, but it lies well away, between 260° and 330°W. The Great Dark Spot (GDS) centered at 23°S, is the most dominant visible feature on Neptune, but at its location during the north-south mapping, approximately 300°W, there is only a slight depression in temperature at 350 cm^{-1}. Perhaps the wave structure at 30°S is forced by the GDS. The meridional profile of zonal winds north of the GDS is not yet well determined, but winds derived from tracking of distinct cloud features blow more strongly eastward as one moves from the GDS toward the south pole (*17*). The GDS may perturb the eastward flow just south of it, generating a train of "lee" waves to the east of it. The amplitude of such a wave train might plausibly decay with distance eastward from the forcing, much as that indicated by the temperature map at 350 cm^{-1}.

Figure 6 displays the meridional distribution of brightness temperatures at 250 and 350 cm^{-1} adjusted to normal viewing, obtained from several scans at higher spatial resolution (approximately 5° at the subspacecraft latitude) that together span latitudes from 85°S to 67°N. The 1σ formal error attributable to random noise in the plotted temperatures is 0.3 and 1.5 K, respectively, at 250 and 350 cm^{-1}. From the figure, the spread in temperatures at any latitude is much larger than the random error, particularly at 250 cm^{-1}, and reflects real variations with longitude. The meridional variation in the 250 and 350 cm^{-1} temperatures are similar, the former being smaller in magnitude. This suggests that the effects of large-scale heterogeneity in cloud opacity at the deeper level is small. Temperatures in the south polar region and the equator are within 1 K of each other. There is a broad band of low temperatures centered at 45°S, as noted in the north-south maps, and the suggestion of another at mid-latitudes in the northern hemisphere. The meridional structure is remarkably reminiscent of that observed on Uranus, which also exhibits mid-latitude temperature minima in both hemispheres (*6, 16*), although there the meridional extent of the minima is smaller.

The visible radiometer data from the scans were fitted by a Minnaert law of the form $I = I_0\mu_0^k\mu^{k-1}$, where μ and μ_0 denote, respectively, the cosines of the emission and solar zenith angles. The best overall fit was obtained with $k = 0.68$. The lower panel of Fig. 7 depicts the variation of I_0 with latitude from one of the scans. There is a pronounced minimum in the reflectivity centered near 55°S, within the latitude range of the temperature minimum. A similar correlation was observed on Uranus (*6*), suggesting that the cooler temperatures are not correlated with enhanced cloud opacity, because denser cloudy regions should be brighter at visible wavelengths.

From the thermal wind equation (*19*), the meridional gradients in temperature along isobars in Fig. 6 imply vertical shears in the prevailing zonal winds. These are depicted

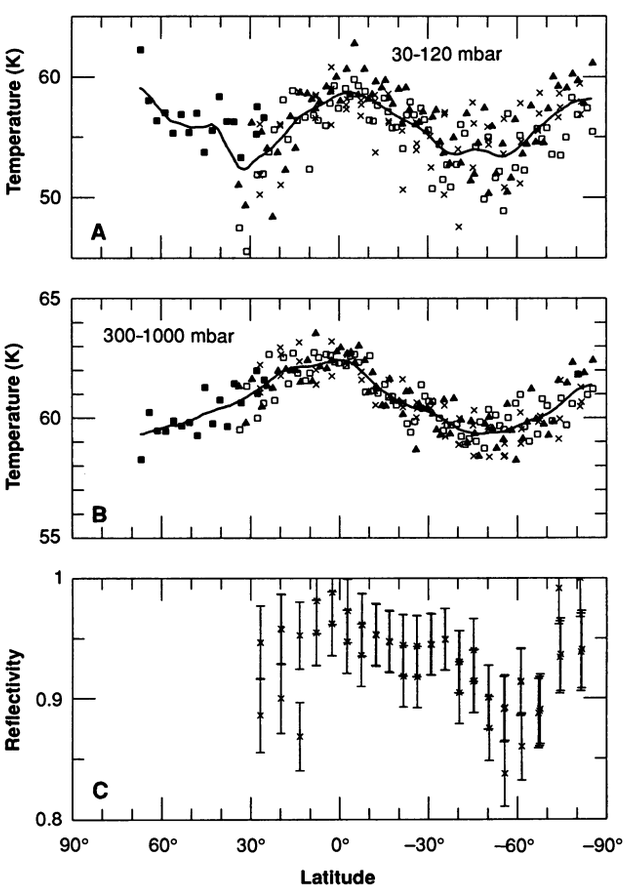

Fig. 6. Latitude scans from several sequences of observations. Relative to a nominal 18-hour rotation period, data obtained at latitudes 30°N to 85°S were centered approximately at 25°W (×'s), 70°W (□), and 120°W (▲), while those at 30° to 67°N (■) were at 240°W. (**A**) Brightness temperatures at 350 cm^{-1}, corrected to normal viewing and equatorial gravity. (**B**) Corrected brightness temperatures at 250 cm^{-1}. The solid curves fitting the temperatures were each generated from two consecutive running means with bins 10° wide in latitude. (**C**) Reflectivity at 0.4 to 1.5 μm in relative units. The reflectivity has been normalized to vertical viewing and vertical illumination by fitting a Minnaert law with $k = 0.68$. The full length of the vertical bars represents the quantization in the radiometer signal.

in Fig. 7. The shears are for the most part positive at low latitudes and negative at high latitudes. On Jupiter, Saturn, and Uranus, comparison of derived thermal wind shears with winds determined from tracking of discrete visible clouds and radio occultation determination of the planetary figure have indicated that the vertical shears are anticorrelated with the zonal winds, in the sense that the winds decay with altitude in the upper troposphere and lower stratosphere (*16, 20, 21*). Hence, on Neptune, one would expect the winds to be eastward at high latitudes and westward at low latitudes, and this appears to be consistent with winds determined by the Voyager imaging investigation (*17*).

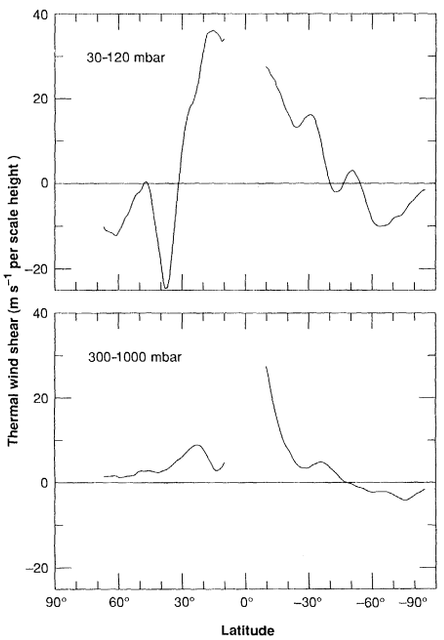

Fig. 7. Zonal thermal wind shears computed from the solid temperature curves in Fig. 6 and then subjected to an additional running mean with bin width of 10° in latitude.

As is the case with the other outer planets, the meridional distribution of temperature on Neptune cannot be solely attributed to radiative effects. Over the pressure range between 300 and 1000 mbar, the radiative relaxation time is comparable to the orbital period of Neptune about the sun (*22*), and the resulting radiatively forced temperature distribution would be a combination of that attributable to the annual mean solar heating and an annual component that lags the temporal-varying solar heating by nearly one season. At the current summer season on Neptune, we would expect both components to produce south polar temperatures that are several degrees cooler than those at the equator. Instead, the observed polar and equatorial temperatures are nearly equal, implying that heat is redistributed dynamically in the troposphere or at deeper levels. The mid-latitude cool bands, reminiscent of Uranus, are not simply explained in terms of radiative forcing, but are more likely attributable to the adiabatic cooling associated with upwelling in the troposphere and lower stratosphere at these latitudes (*16*).

The similarity in the meridional structure of temperature and thermal winds on Neptune and Uranus was unexpected. The obliquity of Uranus (98°) is much larger than that of Neptune (29°), and its internal energy flux is small compared to the flux of sunlight that it absorbs. Evidently, neither the obliquity nor the relative magnitudes of internal and solar heating are strong determinants of the meridional character of temperatures and winds on these planets. The much larger internal heat source on Neptune may account for its more pronounced zonal structure in temperature. The similar zonal wind structure of both planets, with winds subrotating (relative to the approximately 16-hour planetary rotation period) at low latitudes and superrotating at high latitudes, may simply be a manifestation of the tendency of parcels of atmosphere to conserve angular momentum; but why Jupiter and Saturn instead exhibit such strong superrotation at the equator and have such a large number of alternating zonal currents remains unanswered.

Effective temperature. The total thermal emission from a planet is usually expressed in terms of an effective temperature, which is the temperature a blackbody would require in order to emit the same thermal flux. To determine this quantity directly, it is necessary to integrate the planetary emission over all directions and over all wavenumbers. A preliminary estimate of the effective temperature has been made by using an average of 178 spectra obtained on the inbound portion of the trajectory and centered at 30°S with the instrument field of view covering about half of the planetary disk. A temperature profile obtained by inverting this spectrum was used along with a radiative transfer model to extrapolate the measurements to lower wavenumbers to obtain the total thermal emission. In carrying out this calculation, we assumed that the He/H_2 mole fraction ratio was 0.15/0.85. As a consistency check, an analysis was performed on a similar set of spectra obtained on the outbound portion of the trajectory. Sources of error include possible variations of temperature with latitude not properly taken into account by this analysis, uncertainty in the He abundance, and the neglect of possible cloud opacities at low wavenumbers. These considerations lead to an estimate of the effective temperature of 59.3 ± 1 K. For comparison, the most recent estimate from ground-based observations is 59.1 ± 2 K (*23*). If a Bond albedo of 0.31 ± 0.04 is assumed (*24*), an energy balance (ratio of the absorbed solar power to the thermally emitted power) of 2.7 ± 0.3 is obtained. With further analysis of Voyager data, it should be possible to substantially improve on the estimates of both the effective temperature and Bond albedo. The lat-

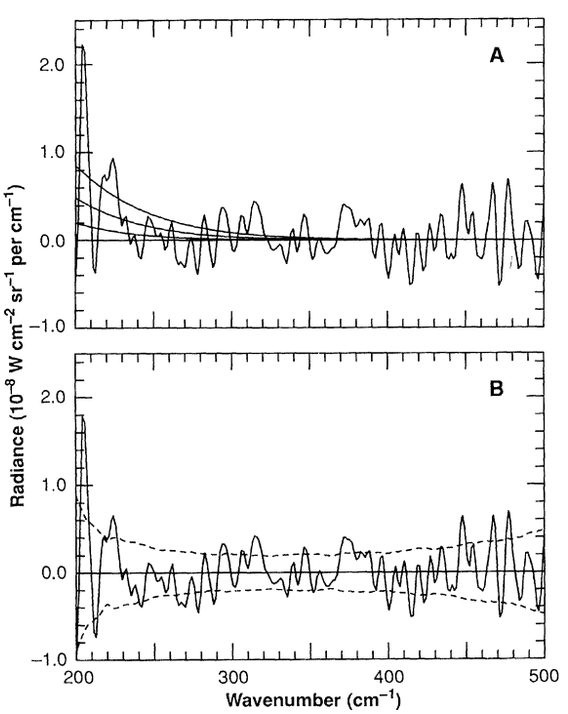

Fig. 8. (**A**) A dayside thermal spectrum of Triton composed of an average of 16 spectra. The smooth curves are Planck functions. For unit emissivity, these correspond to a best-fit surface temperature of 38 K (middle smooth curve) with rough limits of 34 K (lower smooth curve), and 41 K (upper smooth curve); the latter two are based on a residual 5% above the minimum value. (**B**) The residual from the 38 K fit (solid curve) to the data of (A). Also shown is the effective NESR (dotted lines) (the instrument NESR reduced by a factor of 4 to make it compatible with the average of 16 Triton spectra), and its reflection about zero; together, these form an envelope that should define the statistical variation of the residual.

ter will be determined from an analysis of the IRIS radiometer data.

Triton. Triton is an extremely cold object. Few individual IRIS spectra appear to show any thermal signature at all. An average of 16 spectra from the dayside hemisphere (average solar incidence angle, 36°) is shown in Fig. 8A. The spectrum is dominated by noise; nonetheless there appears to be a small signal from Triton at low wavenumbers, an impression corroborated by fitting a Planck function to the spectrum by least squares. The fit was restricted to the region between 200 and 350 cm^{-1}, beyond which little or no signal is expected. The spectral data were weighted inversely as the square of the instrument noise equivalent spectral radiance (NESR) to account for the wavenumber dependence of the noise. The best fit temperature (corresponding to a surface with unit emissivity) is 38 K. Figure 8B shows the residual of the fit, plotted within the noise envelope expected from the NESR; the behavior of the residual appears random. Estimated upper and lower bounds, somewhat arbitrarily defined as the temperatures that result in an increase of 5% in the RMS residual of the fits, are 41 and 34 K, respectively. Planck curves for all of these temperatures are shown in Fig. 8A. For a surface with an emissivity of 0.5 in the spectral region of the fit, the temperature estimate is $T_s = 41^{+3}_{-5}$ K. Temperatures in this range (34 to 41 K) correspond to surfaces with Bond albedos of $A > 0.8$, consistent with the location of the present observations on Triton's bright polar region.

As a result of ground-based measurements, CH_4 and N_2 have been identified on the surface of Triton (*25*). Additionally, both species have been identified in the atmosphere from Voyager Ultraviolet Spectrometer data (*26*). The 38 K surface temperature derived here lies in the β regions of solid CH_4 and N_2 (*27*). From vapor pressure curves for these phases (*28*), equilibrium atmospheres over pure CH_4 and N_2 would have surface pressures of approximately 2×10^{-9} and 20×10^{-6} bars, respectively; the stated temperature limits permit more than an order of magnitude uncertainty in each of these pressure estimates. If any significant amount of solid N_2 is present, however, CH_4 can only be a minor constituent of the atmosphere. Additional effects, such as the presence of solid solutions, mass flow of the atmosphere, and cold trapping, will tend to alter the actual surface pressure from these ideal values.

REFERENCES AND NOTES

1. R. Hanel *et al.*, *Appl. Opt.* **19**, 1391 (1980).
2. R. Hanel *et al.*, *Science* **204**, 972 (1979).
3. R. Hanel *et al.*, *ibid.* **206**, 952 (1979).
4. R. Hanel *et al.*, *ibid.* **212**, 192 (1981).
5. R. Hanel *et al.*, *ibid.* **215**, 544 (1982).
6. R. Hanel *et al.*, *ibid.* **233**, 70 (1986).

6a. The stratosphere denotes that portion of the atmosphere where temperature increases with altitude (that is, with decreasing barometric pressure) above the temperature minimum, or tropopause, near 200 mbar (Fig. 3). The troposphere denotes the atmosphere below the tropopause where temperature decreases with altitude.

7. D. Gautier *et al.*, *J. Geophys. Res.* **86**, 8713 (1981); B. Conrath, D. Gautier, R. Hanel, J. Hornstein, *Astrophys. J.* **282**, 807 (1984); B. Conrath, D. Gautier, R. Hanel, G. Lindal, A. Marten, *J. Geophys. Res.* **92**, 15,003 (1987).
8. D. Gautier, *Philos. Trans. R. Soc. London Ser. A* **325**, 583 (1988).
9. W. Macy and W. Sinton, *Astrophys. J.* **218**, L79 (1977).
10. G. S. Orton, A. T. Tokunaga, J. Caldwell, *Icarus* **56**, 147 (1983).
11. G. S. Orton *et al.*, *ibid.* **70**, 1 (1987).
12. G. S. Orton *et al.*, *ibid.*, in press.
13. P. N. Romani and S. K. Atreya, *ibid.* **74**, 442 (1988).
14. ———, *Geophys. Res. Lett.* **16**, 941 (1989).
15. B. J. Conrath and D. Gautier, in *Remote Sensing of Atmospheres and Oceans*, A. Deepak, Ed. (Academic Press, New York, 1980), p. 611.
16. F. M. Flasar, B. J. Conrath, P. J. Gierasch, J. A. Pirraglia, *J. Geophys. Res.* **92**, 15,011 (1987).
17. B. A. Smith *et al.*, *Science* **246**, 1422 (1989); H. B. Hammel *et al.*, *ibid.* **245**, 1367 (1989).
18. F. M. Flasar *et al.*, *J. Geophys. Res.* **86**, 8759 (1981).
19. J. R. Holton, *An Introduction to Dynamic Meteorology* (Academic Press, New York, 1979).
20. B. J. Conrath and J. A. Pirraglia, *Icarus* **53**, 286 (1983).
21. P. J. Gierasch, B. J. Conrath, J. A. Magalhaes, *ibid.* **67**, 456 (1986).
22. B. J. Conrath, P. J. Gierasch, S. S. Leroy, *ibid.*, in press; B. Bezard, *Adv. Space Res.*, in press.
23. G. Orton *et al.*, *Bull. Am. Astron. Soc.* **17**, 745 (1985).
24. J. B. Pollack *et al.*, *Icarus* **65**, 424 (1986).
25. D. P. Cruikshank and P. M. Silvaggio, *Astrophys. J.* **233**, 1016 (1979); J. Apt, N. P. Carleton, C. D. Mackay, *ibid.* **270**, 342 (1983); D. P. Cruikshank and J. Apt, *Icarus* **58**, 306 (1984); D. P. Cruikshank, R. H. Brown, R. N. Clark, *ibid.*, p. 293; D. P. Cruikshank, R. H. Brown, L. P. Giver, A. T. Tokunaga, *Science* **245**, 283 (1989).
26. A. L. Broadfoot *et al.*, *Science* **246**, 1459 (1989).
27. A. I. Prokhvatilov and L. D. Yantsevich, *Sov. J. Low Temp. Phys.* **9**, 94 (1983).
28. G. N. Brown and W. T. Ziegler, *Adv. Cryog. Eng.* **25**, 662 (1980).

29. We thank A. L. Lane for making computing facilities available to us at the Jet Propulsion Laboratory, J. Piotrowski and W. Smythe for computer system assistance, M. Reisdorf for logistic support, and the Voyager Project staff for their continued support of this investigation. We also thank those at Goddard Space Flight Center who have assisted with data processing, particularly J. Guerber, L. Herath, L. Mayo, M. Silverstein, C. Staub, and J. Tingley.

1 November 1989; accepted 15 November 1989

Ultraviolet Spectrometer Observations of Neptune and Triton

A. L. BROADFOOT, S. K. ATREYA, J. L. BERTAUX, J. E. BLAMONT, A. J. DESSLER, T. M. DONAHUE, W. T. FORRESTER, D. T. HALL, F. HERBERT, J. B. HOLBERG, D. M. HUNTEN, V. A. KRASNOPOLSKY, S. LINICK, J. I. LUNINE, J. C. MCCONNELL, H. W. MOOS, B. R. SANDEL, N. M. SCHNEIDER, D. E. SHEMANSKY, G. R. SMITH, D. F. STROBEL, R. V. YELLE

Results from the occultation of the sun by Neptune imply a temperature of 750 ± 150 kelvins in the upper levels of the atmosphere (composed mostly of atomic and molecular hydrogen) and define the distributions of methane, acetylene, and ethane at lower levels. The ultraviolet spectrum of the sunlit atmosphere of Neptune resembles the spectra of the Jupiter, Saturn, and Uranus atmospheres in that it is dominated by the emissions of H Lyman α (340 ± 20 rayleighs) and molecular hydrogen. The extreme ultraviolet emissions in the range from 800 to 1100 angstroms at the four planets visited by Voyager scale approximately as the inverse square of their heliocentric distances. Weak auroral emissions have been tentatively identified on the night side of Neptune. Airglow and occultation observations of Triton's atmosphere show that it is composed mainly of molecular nitrogen, with a trace of methane near the surface. The temperature of Triton's upper atmosphere is 95 ± 5 kelvins, and the surface pressure is roughly 14 microbars.

BEFORE THE VOYAGER ENCOUNTER, neither Neptune nor Triton had been detected at wavelengths shorter than 1700 Å. Measurements of the ultraviolet (UV) reflection spectrum and the infrared (IR) spectrum of Neptune gave contradictory implications about the distribution of methane (CH_4), ethane (C_2H_6), and acetylene (C_2H_2) in the stratosphere. A temperature of 150 K at the 1-μbar level had been deduced from observations of a stellar occultation. A 1σ upper limit on H Lyman α as low as 180 R (1 R = $10^{10}/4\pi$ photons m^{-2} s^{-1} sr^{-1}) above the background emission was derived from International Ultraviolet Explorer (IUE) observations. Features in Triton's IR reflection spectrum were interpreted as indicating the presence of CH_4